EVS35 Symposium
Oslo, Norway, June 11-15, 2022

Design of Modular Direct-drive Hub Motor with High Torque Density and High Reliability

Shoulun Guo[1], Huichao Zhao[1], Li Zhang[1], Xiangrui Yin[1], Yu Wang[1], Yan Cang[1],
[1]*FAW E-Drive System Sec., Electric Vehicle Development Department, Jilin, China,*
corresponding author: Li Zhang, Email: zhangli1@faw.com.cn

Summary

Direct-drive hub motor is installed in restricted space with requirements of low speed, high torque and high reliability, which brings great difficulties in designing. Aiming at high torque density and high reliability, a multi-unit modular direct-drive hub motor (MMDHM) is designed in this paper, with effective torque density up to 38.1Nm/kg. The influences of different pole-slot ratio, stator structure, magnetizing type of permanent magnets and fixing types of magnets on the electromagnetic performance are studied by means of analytical analysis and finite element method, based on which a high torque density electromagnetic structure is explored. The effectiveness of this motor design and related techniques is verified through finite element simulation and bench test, which provides a reference for the design of direct-drive hub motors with high torque density and high reliability.

Keywords: Multi-unit Modular Hub Motor, Torque Density, Reliability, Pole-slot Ratio, Electromagnetic Performance

1 Header

Hub motor has the advantages of compact structure, convenient control and high transmission efficiency[1], which makes it an important technical direction for new energy vehicle motors. Through various of motors, permanent magnet synchronous motor is the first choice for hub motors because of its high efficiency, high power density and good reliability [2]. At present, researches on hub motors from worldwide scholars mainly focus on the permanent magnet synchronous motor as well [3-5].

The direct-drive hub motor optimizes the chassis structure, cancels the half axis, transmission shaft and other mechanical components, which greatly alleviate the NVH, dynamics and other problems that trouble the chassis. Meanwhile, it significantly improves the transmission efficiency and the flexibility of four-

wheel handling [6-8]. However, operating environment for hub motor is harsh, which proposes extremely high requirements for reliability. Therefore, the common direct-drive hub motor products (such as Protean from England, Schaeffler from Germany, e-Traction from Netherlands, etc.) all adopt the multi-unit modular motor scheme to achieve the fault-tolerant operation [9], and the experiments show that the high-performance hub motor with high reliability can be realized through the fault-tolerant system design[10].The advantages of this design scheme mainly reflect in two aspects: one is the redundant fault tolerance function due to the independence of each unit module, the other is the standardization of the unit module, which can effectively reduce the cost since it's replaceable.

MMDHM designed in this paper has characteristics of high torque density, high reliability, modular design, platform-based control and compact structure, which mainly relies on the following aspects: fractional slot concentrated winding scheme, short ending length of stator winding, high slot-filled factor and small volume. In addition, different units of the modular motors are independent from each other, which makes the system more robust since it can still work well with one unit failure. Three-phase symmetrical alternating current is conducted in the stator windings of each unit, and the rotor is driven to rotate jointly according to the principle of equal torque distribution. The current demand for each unit is 1 / N of the traditional motor (N is the number of units), which can reduce the IGBT selection requirements and increase the layout flexibility.

2 Introduction of MMDHM

2.1 Structure of direct-drive hub motor

The hub motor is directly installed in the wheel hub, as shown in Figure 1, which can realize distributed drive, flexible control and improve the efficiency of the vehicle. According to the powertrain system, the hub motor is mainly divided into deceleration drive type and direct drive type.

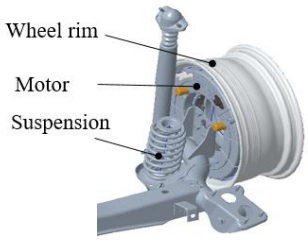

Figure 1: Layout of hub motor

The direct-drive hub motor cancels the gear deceleration mechanism and the rotor is directly installed in the wheel hub to drive the vehicle, as shown in Figure 2, which simplifies the powertrain system structure and improves the transmission efficiency. However, the requirement of torque density is high, and fault tolerance function is essential.

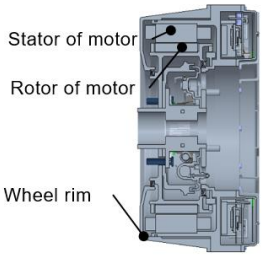

Figure 2: Layout of Direct-drive hub motor

2.2 Structure and principle of the modular motor

Modular hub motor is developed based on the traditional hub motor. Through structural adjustment, the stator of the motor is divided into several modules in the circular direction, and all modules share the same

rotor. Each stator module equips with an independent three-phase AC winding, which is powered by an independent inverter. In order to realize the fault-tolerant operation, the inverter topology of three-phase four-bridge arm is commonly applied [11]. Taking the 4-module hub motor as an example and making the unit motor as 8-pole 9-slot structure, the whole modular hub motor system is shown in Figure 3.

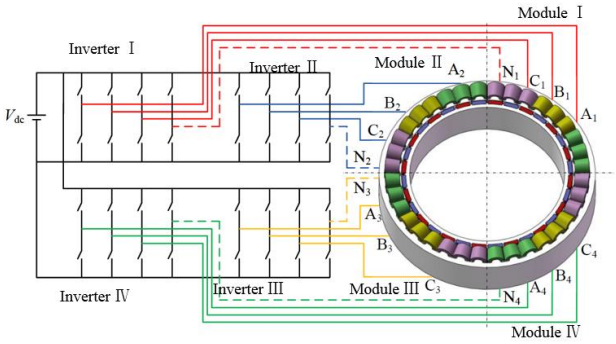

Figure 3: Modular hub motor system topology

As shown in Figure 4, the stator of motor is divided into four modules in the circular direction, and each stator module has an independent three-phase winding connected to the corresponding inverter one by one. Each unit motor can work both independently and jointly [12]. Double layer winding structure is adopted and the phase coils are wrapped around the centralized tooth, which is quite suitable for wheel traction application with restricted axial space [13-14].

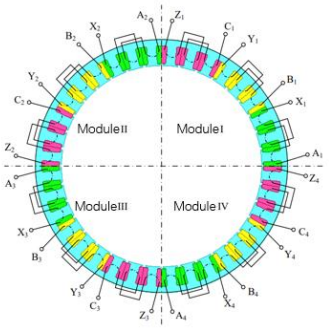

Figure 4: Schematic diagram of modular hub stator

During normal operation, three-phase symmetrical alternating current is passed through the stator windings of each unit motor, and drives the rotor rotation together according to the principle of average torque distribution. Each module generates the magnetic field in the air gap and together contribute the rotating magnetic field in the air gap of the whole hub motor, which has no difference from the traditional permanent magnet hub motor. When stator winding failure occurs (such as an open circuit failure happens on a module), the fault module can be removed and the remaining healthy modules can continue to work in normal level, on this condition, the winding current and output torque of the healthy modules are obviously greater than their normal operating state. Therefore, mostly, in order to reduce the workload and motor loss of the remaining modules, certain fault-tolerant strategies have to be applied to the fault module.

3 Stator Design of MMDHM

3.1 Analysis of pole-slot ratio

The hub motor, as a low speed and high torque motor, more poles are needed according to the relationship between speed and pole number of synchronous motor when the current frequency is constant. Distributed winding increases the number of stator slots, the height of end winding and the volume of the motor, therefore, fractional slot concentrated winding with the slot number of per phase q <1 is a better option. Generally, the poles number is close to the number of slots in this design. To avoid a narrow permanent magnet width, the number of poles per unit motor is generally less than 10. According to the analysis, 10-pole 9-slot, 8-pole 9-slot, 10-pole 12-slot and 8-pole 12-slot are preferred pole-slot ratio. The unit motor

models are shown in Figure 5.

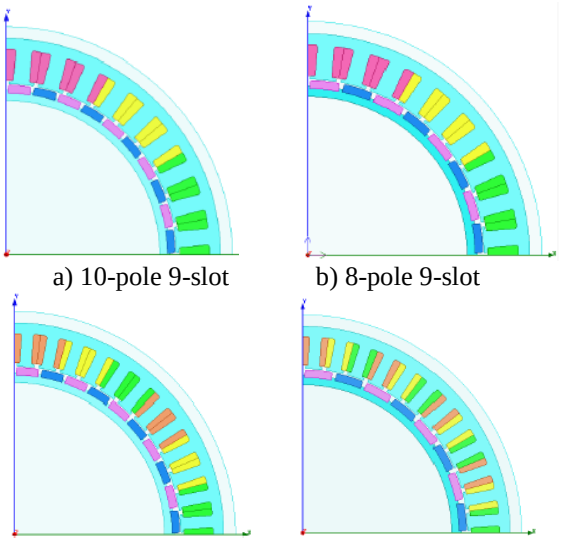

a) 10-pole 9-slot b) 8-pole 9-slot

c) 10-pole 12-slot d) 8-pole 12-slot

Figure 5: Unit motor model

Taking the 10-pole 9-slot scheme as an example, suppose the number of coil turns for each phase winding is Nc, the pole pitch is τ, and phase current is i_A、i_B、i_C. The pulsating magnetomotive force f_A generated by the phase A winding is shown in Figure 6, and its Fourier series is expanded as follows:

$$f_A = \frac{6N_C i_A}{5\pi}\begin{bmatrix} 5\times(-0.0607)cos\left(\frac{2\pi}{10\tau}x\right) \\ +\frac{5}{2}\times 0.1398\cos\left(2\cdot\frac{2\pi}{10\tau}x\right) \\ +\frac{5}{3}\times 0.5774cos\left(3\cdot\frac{2\pi}{10\tau}x\right) \\ +\frac{5}{4}\times 0.9452\cos\left(4\cdot\frac{2\pi}{10\tau}x\right) \\ +\frac{5}{5}\times 0.9452cos\left(5\cdot\frac{2\pi}{10\tau}x\right) \\ +\frac{5}{6}\times 0.5774\cos\left(6\cdot\frac{2\pi}{10\tau}x\right) \\ +\cdots \end{bmatrix} \quad (2\text{-}1)$$

$$=\frac{4}{\pi}qN_C i_A\sum_{V=\frac{n}{5}}^{\infty}\frac{1}{V}k_{dpv}\cos\left(v\frac{\pi}{\tau}x\right)$$

where, n is a positive integer (the same as follows),

v —— harmonic times, *v*=1 is the base wave;

K_{dpv} —— harmonic winding coefficient, expressed as:

$$k_{dpv} = \frac{1}{3}\left[2sin\frac{5v\pi}{9}+\frac{1}{9}sin5v\pi - sin\frac{5v\pi}{3}\right] \quad (2\text{-}2)$$

$$V = \frac{1}{5},\frac{2}{5},\frac{3}{5},\frac{4}{5},1,\frac{6}{5}\ldots$$

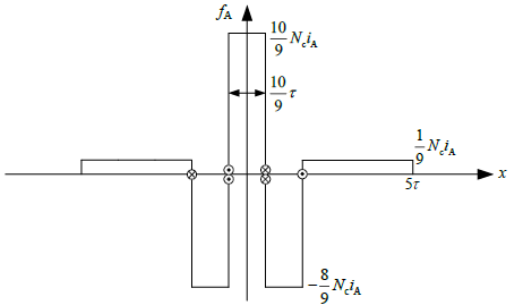

Figure 6: A - phase magnetomotive force distribution of the motor with 10- pole 9- slot

The pulsating magnetomotive force f_A generated by the phase A winding and the pulsating magnetomotive force f_B generated by the phase B winding are spatially staggered, i. e.:

$$f_B = \frac{4}{\pi} qN_C i_A \sum_{V=\frac{n}{5}}^{\infty} \frac{1}{V} k_{dpv} \cos\left[\left(v\frac{\pi}{\tau}(x - \frac{10}{3}\tau)\right)\right]$$

$$= \frac{4}{\pi} qN_C i_A \sum_{V=\frac{n}{5}}^{\infty} \frac{1}{V} k_{dpv} \cos\left(v\frac{\pi}{\tau}x - \frac{10}{3}v\pi\right) \quad (2\text{-}3)$$

$$V = \frac{1}{5}, \frac{2}{5}, \frac{3}{5}, \frac{4}{5}, 1, \frac{6}{5} \ldots$$

Similarly, the pulsating magnetomotive force f_C generated by the phase C winding：

$$f_c = \frac{4}{\pi} qN_C i_A \sum_{V=\frac{n}{5}}^{\infty} \frac{1}{V} k_{dpv} \cos\left[\left(v\frac{\pi}{\tau}x + \frac{10}{3}v\pi\right)\right] \quad (2\text{-}4)$$

$$f_s = \frac{4}{\pi} qN_C \sum_{V=\frac{n}{5}}^{\infty} \frac{1}{V} k_{dpv} \begin{bmatrix} i_A \cos v\frac{\pi}{\tau}x + i_B \cos\left(v\frac{\pi}{\tau}x - \frac{10}{3}v\pi\right) \\ +i_C \cos\left(v\frac{\pi}{\tau}x + \frac{10}{3}v\pi\right) \end{bmatrix} \quad (2\text{-}5)$$

$$\begin{cases} i_A = \sqrt{2}I\cos(\omega t + \varphi) \\ i_B = \sqrt{2}I\cos(\omega t + \varphi - \frac{2\pi}{3}) \\ i_C = \sqrt{2}I\cos(\omega t + \varphi + \frac{2\pi}{3}) \end{cases} \quad (2\text{-}6)$$

ψ——The power factor angle;

put ψ into （2-5）：

$$f_s = \frac{6\sqrt{2}}{\pi} qN_C I \sum_{V=\frac{n}{5}}^{\infty} \frac{1}{V} k_{dpv} \cos\left[v\frac{\pi}{\tau}x \pm (\omega t + \varphi)\right] \quad （\text{n is not divided by 3 }） \quad (2\text{-}7)$$

where, the selection of "±" and the harmonic number are correlated: when n=1, the minus sign is taken, the sign of n=3k + 1 and n=3k-1 is opposite (*k* is a positive integer, the same as follows).

From Equation (2-7), it can be seen that the corresponding synthetic harmonic magnetomotive force is 0 when n=3k. Also, when n=3k + 1, the amplitude of three-phase synthetic harmonic magnetomotive force is 1.5 times of its counterpart of single-phase, besides, the rotating direction of harmonic magnetomotive force is opposite compared to that when n=3k-1.

According to equation (2-2), the harmonics winding factors of the 10-pole-9-slot scheme (not considering the multiple harmonics of 3 and 3) can be derived. Setting the base wave as 1, the spectrums of the four pole-slot ratio schemes are shown in Figure 7.

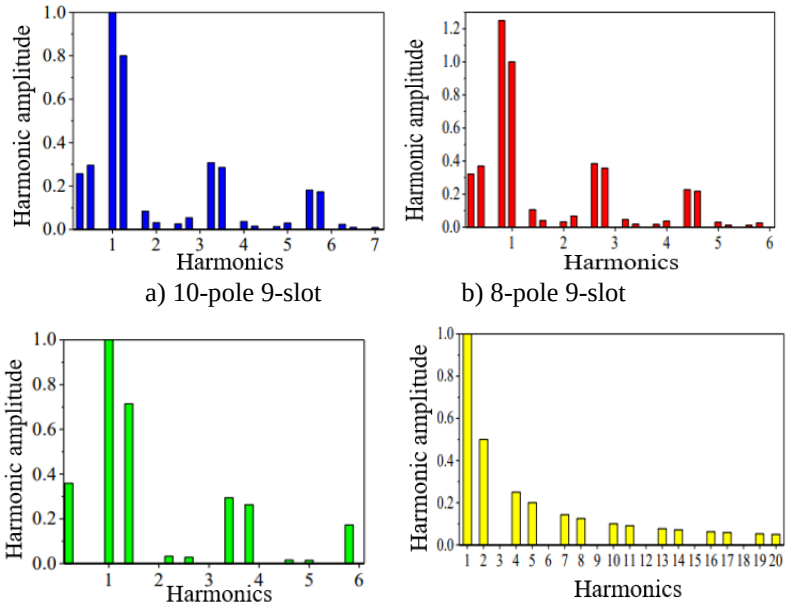

Figure 7: Magnetomotive force spectrum

Compared with the distributed windings, the magnetic electromotive force produced by the fraction slot winding often contains rich harmonics [16]. As a result, the rotor core loss of fractional slot winding motor is generally larger than that of distributed winding motor. From the perspective of rotor core loss, the 0.8th harmonic amplitude of the 10-pole 9-slot even exceeds the base wave, which will produce a large eddy current loss, and the base wave component dominates in the frequency spectrum of the 8 pole-12 slot, which is similar to the integer slot winding, and the eddy current loss is correspondingly small.

Performances of unit motors in four different pole-slot ratio schemes are analyzed through finite element simulation. To set the pole-slot ratio as a single variable by keeping the same electric load and magnetic load, the number of conductors per slot is 96 for 9-slot unit motor and 72 for 12-slot unit motor. And the following three working conditions are selected for finite element simulation. The simulation working conditions are shown in Table 1.

Table 1: Different simulation conditions

Condition	Speed[r/min]	Current[A]
No-load	1300	0
Normal load	700	12
Full load	450	40

No-load back EMF of the unit motor under no-load condition is shown in Figure 8. No-load back EMF waveforms show flat top trend, the main harmonic component of 10-pole 9-slot, 9-pole 8-slot and 10-pole 12-slot schemes is 3, while 5 and 7 harmonics are more obvious for 8-poles 12-slot scheme. Since the base wave winding factor of the 8- pole 12-slot is the lowest, the base wave component of the no-load back EMF is also the smallest, while the base wave component of the 10-pole 9-slot and the 8-pole 9-slot unit motor is large.

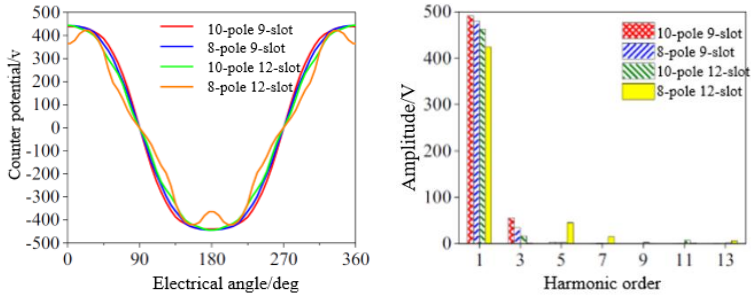

Figure 8: No-load back EMF with different pole-slots ratio

The torque of the hub motor under the full load condition with different pole-slot ratio are shown in Figure 9. And the torque of unit motor with 10-pole 9-slot and 8-pole 9-slot are higher, and that with 10-pole 12-slot is lower, and the torque is smallest with largest torque fluctuation of the unit motor with 8-pole 12-slot.

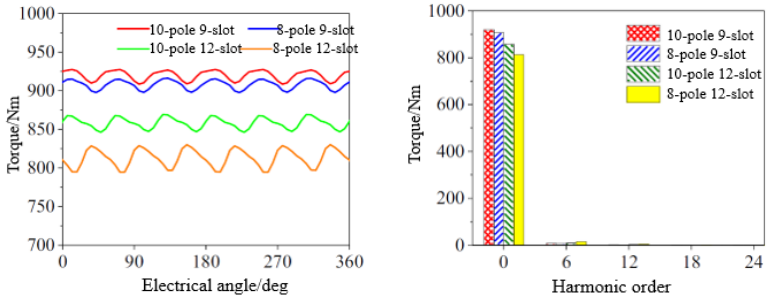

Figure 9: Torque with different pole-slots ratio
Oscillogram(left), Power Spectrum(right)

Under the general load and full load conditions, the permanent magnet eddy loss of the unit motor under different pole-slot ratio shown in Figure 10.As can be seen in the figure, the motor eddy loss is the largest at the 10-pole 9-slot and the 8-pole 12-slot.This is because the 8-pole 12-slot winding has the characteristics of integer slot winding, the magnetic momentum is mainly base wave component, while the 10-pole 9-slot winding has more harmonic components, and the 4 and 5 harmonic component is even higher than the base wave, resulting in large eddy loss. The eddy loss will increase the permanent magnet temperature and decrease the permanent magnet performance. Therefore, considering the motor torque output capacity and reducing the permanent magnet demagtization risk, the unit motor should adopt 8-pole 9-slot structure.

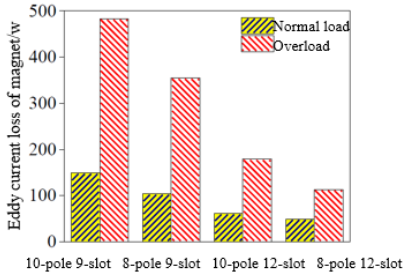

Figure 10: Permanent magnet eddy loss with different pole-slots ratio under general load and full load condition

3.2 Selection of stator structure

Mostly, Stator core adopts a uniform tooth structure, but for modular permanent magnet hub motors, in order to achieve high fault tolerance characteristics, isolation teeth can be added between different unit motor stator to achieve magnetic isolation and thermal isolation between the modules. The motor stator core and its magnetic field distribution are shown in Figure 11.

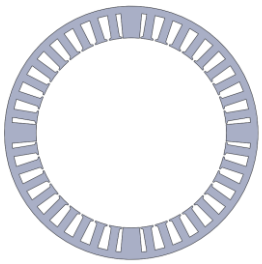

（a）Stator with non-uniform tooth structure

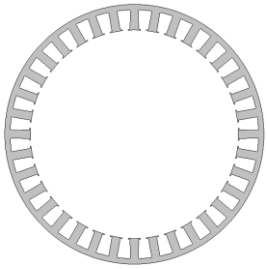

(b）Stator with uniform tooth structure

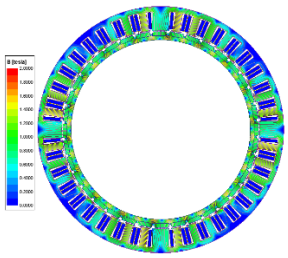

（c）Magnetic field distribution of non-uniform tooth structure on no-load condition

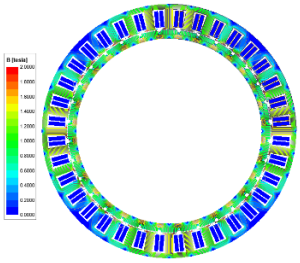

(d）Magnetic field distribution of uniform tooth structure no- no-load condition

Figure 11: Comparison of non-uniform tooth and uniform tooth motor

The comparison of No-load back EMF at 1300 r/min is shown in Figure 12. The No-load back EMF of the motor with non-uniform tooth is relatively small, because when the stator adds isolation teeth, the number of rotor poles increases from 32 to 36 poles, and the width of the permanent magnet becomes narrow, and the magnetic flux at each pole decreases accordingly, resulting in the decrease of the No-load back EMF.

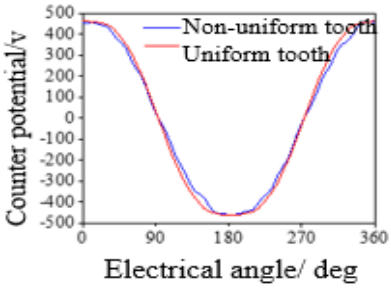

Figure 12: No-load back EMF with uniform tooth and non-uniform tooth

As shown in figure13, the no-load back EMF of non-uniform tooth motor is relatively small, and the torque is reduced by about 10% compared with uniform tooth. As the isolation teeth occupy a large space, the rest of the teeth will narrow, which leads to the saturation of the stator core during the full load condition, and the full load capacity of the motor also decreases.

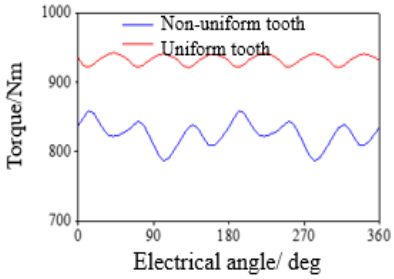

Figure 13: Torque with uniform tooth and non-uniform tooth

Compared with the motor with uniform tooth, it can be seen that the motor with non-uniform tooth has the following characteristics:

1. It has high fault tolerance because each unit can realize magnetic and thermal isolation;

2. It has low electromagnetic load capacity and high saturation due to the existence of isolation teeth, which is not conducive to achieving high torque density.

To pursues high torque density, the uniform tooth stator is chosen in this paper. Therefore, the non-uniform tooth has great research value for achieving high fault tolerance characteristics.

4 Rotor Design of MMDHM

In view of the small size and space characteristics of the Direct-drive hub motor, surface-mounted magnet is selected rather than the inner-mounted. And the types of magnet fixation and its magnetization have been analyzed before the final design.

4.1 Analysis of magnetization features

There are mainly three magnetization types for PMs in a motor, vertical magnetization, horizontal magnetization and Halbach magnetization, and vertical magnetization is mostly used for the IPMSM. For Halbach magnetization the permanent magnets are arranged in different magnetization directions according to a specific rule to gather the magnetic line on one side and weaken the magnetic line on the other side, so as to obtain an ideal one-side magnetic field [15]. This type of magnetization can make the flux distribute more sinusoidal in the air gap, help to reduce the harmonic components of the magnetic flux and improve the magnetic load of the motor. But its processing process is more complex, and the process cost is relatively high. The performance of vertical magnetization and Halbach magnetization are investigated in this paper. And the simulation results of vertical magnetization and Halbach magnetization on no-load and full load conditions are shown in Fig. 14 and Table 2.

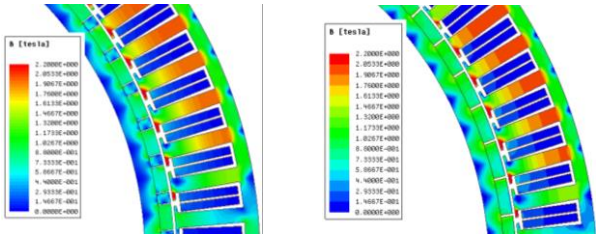

(a) Halbach magnetization (b) Vertical magnetization

Figure 14: Distribution of magnetic density under different magnetizing modes

Table 2: Simulation results of vertical magnetization and Halbach magnetization

Parameters	Halbach magnetization	vertical magnetization
Size of Magnet /mm	(9.9+4.1)*5*70	14*5670
Peak torque/Nm	754.8	743.1
Torque ripple/%	2.85	4.15
Cogging torque /Nm	5.1	4.7

Motor with Halbach magnetization has no obvious advantages according to the results. And considering Halbach magnetization process is much difficult than that of vertical magnetization, so the vertical magnetization is the choice of the final design.

4.2 Analysis of fixing types of magnets

Two fixing types of magnets have been analyzed in this paper in order to ensure the effective fixation of the magnet, one way is to be fixed by outer sheath, the sheath material is Cr17Ni4Cu4Nb and its thickness is 0.5mm; the other way is to be embedded in the dovetail groove as shown in Figure 15.

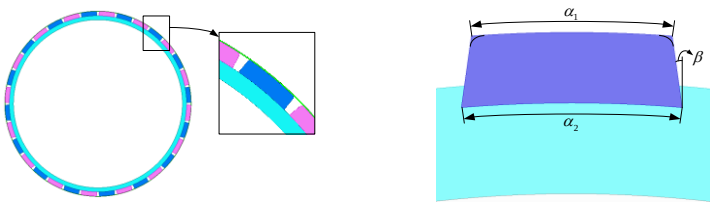

(a) Magnet fixed with sheath (b) Magnet embedded in the dovetail groove

Figure 15: Fixing types of magnets

On the condition of no-load at 1300 r/min and on the load condition at 40A current, the motor is of lower No-load back EMF and lower torque when magnetic is fixed with sheath, which shows in Figure 16-17.

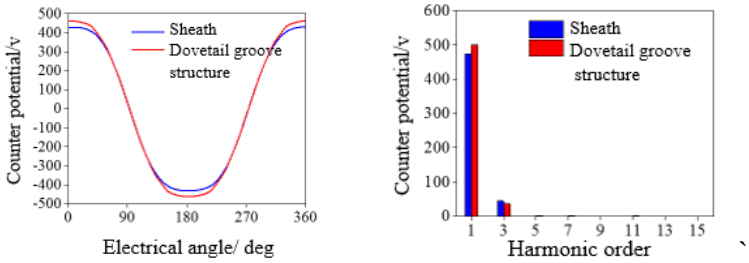

Figure 16: No-load back EMF with two different fixing types of magnets
Oscillogram (left), Power Spectrum (right)

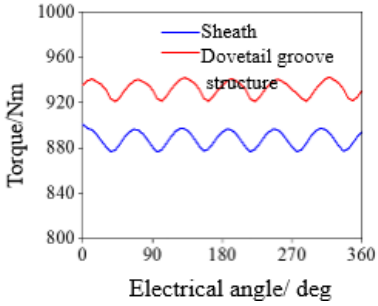

Figure 17: Torque curves with two different fixing types of magnet under load condition

The actual electromagnetic air gap of the motor with outer sheath is larger while remaining the same physical gap between these two type motors, which weakens the air gap magnetic field for the motor with outer sheath, furthermore, the no-load back EMF and output torque reduces accordingly. In order to improve the no-load back EMF and output torque, the amount of permanent magnet has to be increased, so as to the volume and weight of the motor. In contrast, the rotor adopts the dovetail groove structure can not only meet the rotor strength requirements, but also improve the motor torque density. Therefore, the rotor with dovetail groove structure is applied in the final design.

5 Simulation and Bench test

5.1 Simulation

The final design is of 32-pole 36-slot with four modules, and its unit motor is of 8-pole 9-slot as shown in figure 18. The main target specifications and design parameters of MMDHM are as shown in table 3.

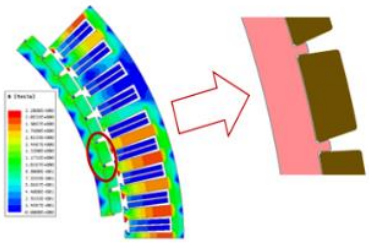

Figure 18: Unit motor of MMDHM
Table 3: Main target specifications and design parameters of the motor

Figures	Target specifications	Design parameters
Voltage /V	700	700
Total phase current/A	≤160	132
Outer diameter of stator/mm	360	360
Max speed/rpm	1300	1300
Length of core/Nm	≤60	60
Peak torque/Nm	≥700	720
Peak power/kW	≥50	58
Max efficiency/%	≥95	95.5
Cogging /Nm	≤1	0.34
torque density /Nm/kg	≥38	38.1

As shown in Table 3, the final design of MMDHM meets the expected targets with the highest efficiency up to 95.5%, and the torque density as high as 38.1Nm/kg. Meanwhile, because of the unit motor characteristics of 8-pole 9-slot, the cogging torque is only 0.34 Nm. The simulation external characteristics of the motor is as shown in Figure 19.

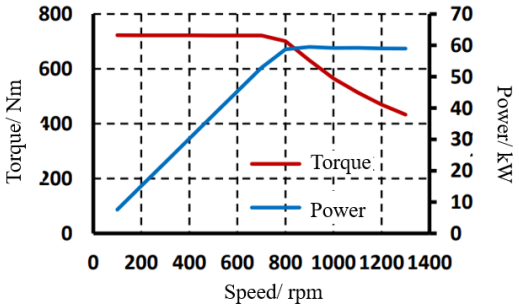

Figure 19: external characteristics of the motor simulation

Simulation of efficiency map is shown in Figure 20, the area greater than 85% efficiency accounts for more than 80% of the whole working area.

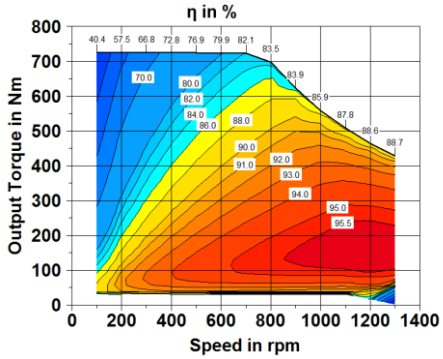

Figure 20: efficiency map of the motor simulation

5.2 Bench test

Bench test under no-load condition and full load condition have been taken for verifying the motor as shown in figure 21, and the results are analyzed below.

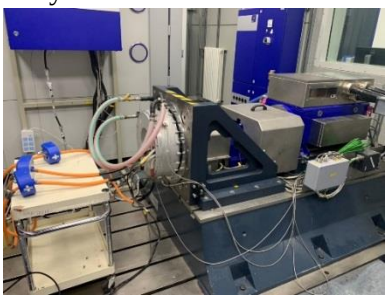

Figure 21: Bench test

5.2.1 Analyze of no-load back EMF

The no-load back EMF of the motor at 500 r/min at 20℃ is shown in Figure 22. Uab, short for the no-load back EMF of the phase U and phase V, is 855.4V at the maximum speed of 1300 r/min, which is 2.19% larger compared with 837V of the simulation result as shown in Figure 23. And it is mainly due to the performance deviation of permanent magnet and motor processing deviation.

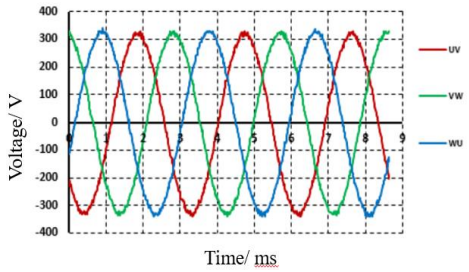

Figure 22: No-load back potential of the motor at 500 r/min at20℃

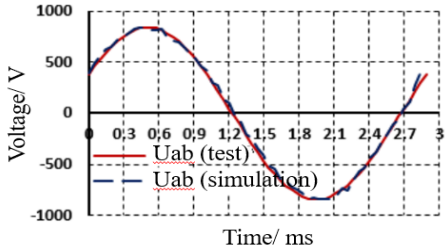

Figure 23: Comparison of simulation and test results of no-load counter potential

5.2.2 Comparison of efficiency data

The comparison of simulation and test results of the efficiency map is shown in figure 24.

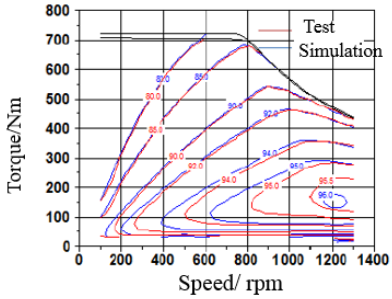

Figure 24: Comparison of simulation efficiency and test efficiency

The highest efficiencies for simulation and test were 96.2% and 95.6% based on the efficiency data, and the deviation is 0.6%. In addition, to derive deeper difference on the cycle efficiency, an efficiency zone equivalence method based on WLTC cycle conditions is applied, and the equivalent classification is conducted for each zone through the ratio of energy efficiency and typical points are used to represent the whole energy efficiency, as shown in table 4.

Table4: Comparison of simulation efficiency and test efficiency by efficiency zone equivalence method based on WLTC cycle conditions

Average speed/ rpm	Average torque /Nm	Ratio of Power consumption	Simulation efficiency/ %	Test efficiency/ %
126	68	0.02	89.51	87.2
129	210	0.03	79.70	75.8
294	118	0.17	92.46	92.1
492	69	0.19	94.31	93.4
699	58	0.14	94.12	93.3
975	93	0.46	95.35	94.7

The maximum deviation between the test efficiency and simulation efficiency of the same equivalent working conditions is 3.9%, and the minimum deviation is 0.36%, which are highly matched. The deviation happens mainly due to the change of the bench accuracy and the temperature during the test.

The bench test objectively shows the actual output capability of the motor, by which not only realized the effective test of production and processing, but also corrected the selection of parameters in the simulation, which provides a reference for the development of the hub motor.

6 Conclusion

A multi-unit modular Direct-drive hub motor is designed in this paper to satisfy the tough requirements, and the effective torque density reaches 38.1Nm/kg. The main conclusions are as follows:

(1) Through theoretical analysis and finite element simulation verification, it shows that the 8-pole 9-slot motor scheme is of lowest eddy current loss compared to 10-pole 9-slot and 10-pole 12-slot; the 8-pole 9-slot motor scheme is of largest torque density compared to 8-pole 12-slot and 10-pole 12-slot, therefore, the 8-pole 9-slot scheme is determined.

(2) Through the multi-dimensional analysis on torque density, no-load back EMF and torque ripple, the uniform toothed stator has better performance.

(3) Through multi-dimensional analysis of output torque, torque ripple, cogging torque, manufacture difficulty and cost, dovetail slot rotor structure with vertical magnetization is with greater advantages.

(4) Through comparison of simulation and bench test, the design technique of MMDHM is validated, also the effectiveness of the efficiency zone equivalence method based on WLTC cycle condition is verified.

7 Referencing

[1] Kazak A N, Filippov D M. Development of In-wheel Motor for Vehicles [C]//2019 IEEE Conference of Russian Young Researchers in Electrical and Electrical Engineering. Institute of Electrical and Electrical Engineers，2019:1406-1408.

[2] Kong Chuiyi，Dai Ying，Luo Jian. Development Status and Trend of In-Wheel Motor Technology for Electric Vehicles[J]. Motor control and application，2019，46（2：101-108，113.

[3] Wang J B, Atallah K, Zhu Z Q, et al. Modular Three-Phase Permanent-Magnet Brushless Machines for In-Wheel Applications[J]. IEEE Transactions on Vehicular Technology, 2008, 57(5): 2714-2720

[4] Yang Y Y，Rahman Mm，Lambert T，et al. Decelopment of an External Rotor V-Shape Permanent Magnet Machine for E-Bike Applicationp[J]. IEEE Transactions on Energy Concersion，2018,33(4)：1650-1658.

[5] Sui Huaxing. Research on the hub of electric bicycle based on disc ironless motor[J]. Electric bicycle, 2018, 12(3)：41-44.

[6] Chu Wenqiang，Application and Developing Trend of In-Wheel Motors Home and Abroad[J]. [J]. Micromotors，2017，40(9)：77-81

[7] Li Yinyin. Design and research of direct-drive in-wheel motor for electric vehicle[D]. Zhejiang University，2017

[8] Huang Shurong, Xing Dong, Xu Wei. Overview of Key Technologies of In-wheel Motors for New Energy Electric Vehicles[J]. new industrialization，2015，5(2):27-32.

[9] Wei Dongxin, Research on Open-Circuit Fault Tolerant Control Strategies of Modular Permanent

Magnet Synchronous Hub Motor [D]. Harbin：Harbin Institute of Technology，2018.

[10] Ifedi C J，Mecrow B C，Brockway S T M，et al. Fault-Tolerant In-Wheel Motor Topoligies for High-Performance Electric Vehicles[J]. IEEE Transactions on Industry Applications， 2013， 49(3):1249-1257

[11] Gao H Y,Bai X F,Li W L.Redundant Control Technology based on Four-leg Topology of Permanent Magnet Synchronous Motor. 2015 3rd International Conference on Computer and Computing Science. 2015

[12] Yu Di. Research on Control Strategy of Modular Permanent Magnet In-Wheel Motor[D]. Harbin: Harbin Institute of Technology，2017.

[13] Luo Ling, Mei Kangyuan. Design of PM Brushless Hub Motor with Fractional Ratio of Slot and Poles [J]. Micromotors. 2011 (05)

[14] Tan Jiancheng. Study on Combination Law of Slot Pole Number of Fractional Slot Concentrated Winding of Three-Phase Brushless DC Motor (Part 1) [J]. Micromotor. 2007 (12)

[15] Zhang Yiming, Qiao Dezhi, Gao Junxia. Research Status and Application of Halbach Array Permanent Magnets[J]. Analytical Instruments, 2010, No.2.

[16] Tang Renyuan. Modern Permanent Magnet Machines [M]. Bei Jing：China Machine Press，2015.

Presenter Biography

Shoulun Guo, male, born in 1988, master graduate from Harbin Institute of Technology, engineer, majoring in electromagnetic design of EV/HEV motors, NVH development and performance development of EV drive system.

Huichao Zhao, male, born in 1975, master graduate from Jilin University. He is President of the New Energy Development Institute of FAW, China. His research interests include design of electric drive powertrains for Electric Vehicle and Hybrid Electric Vehicle. Huichao Zhao is a member of China Electrotechnical Society, a member of IGBT Technology Innovation and Industry Alliance in China, and a senior advisor of Automotive Digest. He is the main writer of electric drive system part of Made in China 2025.

Li Zhang, female, born in 1988, master graduate from Harbin Institute of Technology, engineer, majoring in electromagnetic performance design optimization of new energy vehicle motors.

Xiangrui Yin, male, born in 1992, master graduate from Harbin Institute of Technology, engineer, majoring in electromagnetic performance design optimization and vibration & noise optimization of new energy vehicle motors.

Yu Wang, male, born in 1976, bachelor graduate from Tianjin University, Senior Director of Electric Drive System Institute of FAW, China, majoring in new energy vehicle motors.

Yan Cang, Male, born in 1989, bachelor graduate from Zhejiang University, engineer, majoring in mechanical design of new energy vehicle motors.